

# Programmable High-Resolution Spectral Processor in C-band Enabled by Low-Cost Compact Light Paths

Zichen Liu <sup>1</sup>, Chao Li <sup>2</sup>, Jin Tao <sup>3</sup> and Shaohua Yu <sup>3,\*</sup>

<sup>1</sup> Wuhan National Laboratory for Optoelectronics, Huazhong University of Science and Technology and Wuhan Research Institute of Post and Telecommunication, Wuhan 430074, China; zchliu@wri.com.cn

<sup>2</sup> Information Materials and Intelligent Sensing Laboratory of Anhui Province, Institutes of Physical Science and Information Technology, Anhui University, Hefei 230601, China; chao.li@ahu.edu.cn or seven\_chao0620@163.com

<sup>3</sup> National Information Optoelectronics Innovation Center, Wuhan Research Institute of Posts and Telecommunications, Wuhan 430074, China; taojin@wri.com.cn

\* Correspondence: shaohua.yu@cict.com

Received: 2 October 2020; Accepted: 3 December 2020; Published: 7 December 2020



**Abstract:** The flexible photonics spectral processor (PSP) is an indispensable element for elastic optical transmission networks that adopt wavelength division multiplexing (WDM) technology. The resolution and system cost are two vital metrics when developing a PSP. In this paper, a high-resolution  $1 \times 6$  programmable PSP is investigated and experimentally demonstrated by using low-cost compact spatial light paths, which is enabled by a 2 K (1080p) liquid crystal on silicon (LCoS) and two cascaded transmission gratings with a 1000 line/mm resolution. For each wavelength channel, the filtering bandwidth and power attenuation can be manipulated independently. The total insertion loss (IL) for six ports is in the range of 5.9~9.4 dB over the full C-band. The achieved 3-dB bandwidths are able to adjust from 6.2 GHz to 5 THz. Furthermore, multiple system experiments utilizing the proposed PSP, such as flexible spectral shaping and optical frequency comb generation, are carried out to validate the feasibility for the WDM systems.

**Keywords:** programmable; photonics spectral processor (PSP); liquid crystal on silicon (LCoS); high-resolution and low-cost; optical frequency combs (OFC)

## 1. Introduction

With the exponential growth of communication traffic driven by high-definition TVs, online social networks, cloud computing and the Internet of things (IoT), there is an unprecedented requirement on high-capacity data transmission over optical transport networks [1]. The next generation wavelength division multiplexing (WDM) optical networks are required to be elastic. They must be capable of dynamically and efficiently allocating a flexible amount of optical spectra with different modulation baud rates to separated outputs [2]. To maximize the network efficiency with limited fiber bandwidths, a new G.694.1 standard has been established by the International Telecommunication Union. The new provision has a 12.5 GHz bandwidth slot width, which helps to reduce the optical protective band in order to improve the transmission efficiency in the previous G.692 specification. Moreover, advanced modulation techniques such as multi-carrier orthogonal frequency division multiplexing (OFDM) and single-carrier Nyquist shaping combined with high-order quadrature amplitude modulation (QAM) formats are expected. This scheme is expected to result in promising solutions for realizing highly-efficient future super-channel optical networking where multiple carriers are very close to each other with minimal guard-bands [3,4]. Both programmable high-resolution photonics spectral processors (PSPs) and wavelength selective switches (WSSs) can switch optical signals flexibly.

Benefiting from the adoption of PSP and WSS, flexible-grid reconfigurable optical add/drop multiplexers (ROADM) realize the functionalities of the supporting programmable channel bandwidth and provide a fine wavelength tuning of sub-GHz, i.e., 6.25 GHz [5].

PSP provides a higher resolution than WSS, excluding the fact that they achieve the same functions of filtering and optical power manipulation. To achieve cost efficiency and a satisfactory performance, both WSSs and PSPs need to consider the factors such as cost, volume, and insertion loss (IL). It has been proposed that one replaces the expensive  $M \times N$  WSS with multiple  $1 \times K$  WSSs for the partially directional high-degree ROADMs [6]. Generally, researchers hope to increase the number of ports and the degree of integration by sharing an expensive liquid crystal on silicon (LCoS) device and bulk optical components [7–9]. It is believed that designing a high-resolution  $1 \times K$  PSP with lower cost and compact size can be helpful in decreasing the total cost of an  $M \times N$  PSP, since it is compatible with the multiple integration solution demonstrated in [8]. Due to its multiple functionalities, the programmable PSP can be implemented in future ultra-high capacity optical systems and networks.

Generating the shape of the arbitrary spectrum: The generation of a variable bandwidth and arbitrary spectrum shape is important in the implementation of the system, such as channel shaping, channel selection and channel gain equalization. For example, by programming the shape of the filter into PSP, one can study the cascading effect of the filter on the transmission quality.

Generating proper optical frequency combs: The generation of controllable optical combs is the key point in optical WDM transmission systems. It requires the PSP to have the high-resolution capability of attenuating the optical power arbitrarily and creating special spectral lines even if they have independent shapes with modulation.

Currently, the spatial light modulator (SLM) utilizing LCoS (LCoS-SLM) is the most competing technique adopted in the design of multiple port WSSs [10–14]. LCoS device combing with gratings can be further developed as programmable PSP for processing optical spectrum resources [15]. Recently, demonstrations have been reported on generating a reconfigurable PSP [15–18]. In [15], Gao et al. proposed and demonstrated a flexible PSP based on a 4K LCoS with a minimum pixel spacing of 3.74  $\mu\text{m}$ . However, they just developed a one-input one-output filter with an achieved minimum 3-dB bandwidth of 10 GHz. Moreover, the price of the employed high-resolution LCoS-SLM is quite expensive. In 2019, their group also demonstrated a reconfigurable PSP, that provided a minimum bandwidth of 12.5 GHz in the C-band by using digital micro-mirror devices. The major drawback is that the achieved tuning resolutions of the center wavelength and IL of this filter are large, being 4.125 GHz (0.033 nm) and 10 dB across the whole C-band, respectively [16]. Rudnick et al. proposed the use of a waveguide grating router (WGR) to implement a high-resolution PSP with a 0.8 GHz optical resolution [17]. However, the achieved free spectral range is just 200 GHz. Besides, to obtain such a high-resolution, large delays within the WGR are required while still maintaining phase accuracy at the output, which is beyond standard fabrication tolerances. Employing spatial light paths, WSS with a high input and output ports has been demonstrated in [8,19,20]. In order to better meet the future development of high-resolution PSP, the designed spatial light paths are required to be compact and have a low IL.

In this paper, we propose low-IL and compact spatial light paths in order to develop a high-resolution low-cost programmable PSP. The concrete scheme is realized by using a 2K LCoS-SLM (The price of 2K LCoS-SLM is less than half of 4K LCoS-SLM) and two cascaded diffraction gratings with a 1000 line/mm resolution. We experimentally demonstrate a  $1 \times 6$  PSP operating across the entire C-band. The achieved minimum 3-dB bandwidth is 6.2 GHz and the largest coverage can be extended to the full C-band of 5 THz spectra by a tuning step of 3.1 GHz. The best and worst ILs for all six ports are less than 6 dB and 9.5 dB, respectively, with about a 1-dB wavelength-dependent loss (WDL). Moreover, arbitrary spectral amplitude manipulations with more than a 20-dB suppression ratio have been experimentally obtained. Compared with the optical signal generator based on commercial products, our proposed method has a better performance for the minimum bandwidth setting and spectral suppression ratio for optical frequency comb (OFC) generation. The achieved results reveal

that it is feasible to develop such a programmable and high-resolution PSP by employing commercial cheap devices and compact spatial light paths and to further implement them in a cost-efficient  $M \times N$  PSP. This is because the employed optical components and the designed compact light paths help to improve the wavelength separation ability, while this does not affect the design of the number of input and output ports of the WSS.

## 2. Materials and Methods

### 2.1. Principle of Operation

When designing an optical filter, the center wavelength tuning resolution  $R_{res}$  and minimum spectral bandwidth  $B_{min}$  are the two key specifications that need to be taken into consideration. In this paper, by using two cascaded gratings, the proposed method and light path contribute to achieving a wide dispersed spectrum in space, finally cover larger working length on the LCoS chip. Based on [15], the larger spot size across the  $y$ -axis, the smaller the spectral bandwidth. Figure 1 illustrates the operation principle of the LCoS-based programmable PSP. The near parallel input beam is injected onto the transmission gratings. The employed gratings (PING-Sample-083) with a 1000 line/mm resolution feature a high efficiency and high tolerance to the illumination angle of incidence. With a 90% diffraction efficiency, the incidence angle range can be tuned from  $46^\circ$  to  $54^\circ$  [21].

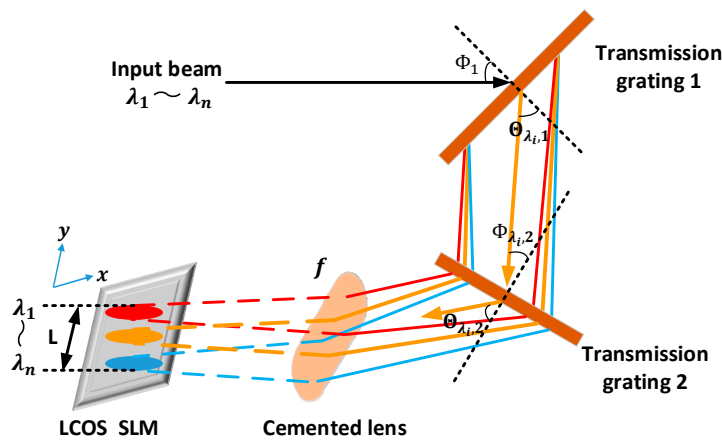


**Figure 1.** Operation principle of the liquid-on-crystal (LCoS) based programmable PSP using dual-grating.

In the experiment, the incidence angle to the first grating is set at the optimal value of  $49.9^\circ$ , which means that  $\Phi_1$  equals to  $49.9^\circ$ . When the input optical beam passes through the transmission grating 1, the wideband signals ( $\lambda_1 = 1530 \text{ nm} \sim \lambda_n = 1570 \text{ nm}$  in the experiment) are spread into angularly separated wavelengths. The first-order diffraction angle of the transmission grating 1 follows the grating equation as follows [22]

$$\sin \Theta_{\lambda_{i,1}} + \sin \Phi_1 = \frac{\lambda_i}{d} \quad (1)$$

where  $\Theta_{\lambda_{i,1}}$  represents the diffraction angle of the input optical beam with the wavelength of  $\lambda_i$  transmitted after the first grating.  $d$  is the groove width of the gratings, which is  $1 \mu\text{m}$ . According to Equation (1), the diffraction angle difference for the wideband signal can be calculated by  $\Delta\Theta_1 = \Theta_{\lambda_{n,1}} - \Theta_{\lambda_{1,1}} = 53.6^\circ - 49.9^\circ = 3.7^\circ$ . Then the angular separated lights are transformed into the second transmission grating. The optimal incidence angle of  $49.9^\circ$  is assigned to the central wavelength of  $1550 \text{ nm}$ . Thus, the incidence angles for  $1530 \text{ nm}$  and  $1570 \text{ nm}$  are set as  $49.9^\circ + 3.7^\circ/2 = 51.75^\circ$  and  $49.9^\circ - 3.7^\circ/2 = 48.05^\circ$ , respectively. The calculated diffraction angle difference after traveling through the second grating is  $\Delta\Theta_2 = \Theta_{\lambda_{n,2}} - \Theta_{\lambda_{1,2}} = 55.7^\circ - 48.1^\circ = 7.6^\circ$ . Therefore, compared with

the single grating, the dispersed angle in space is doubled. The transmission grating 2 and LCoS chip are arranged at the front and back focal planes of the cemented lens, whose focal length is  $f = 100$  mm. The position distribution  $L$  along the  $y$ -axis on the LCoS chip is further expressed as

$$L = 2f \cdot \tan(\Delta\Theta_2/2) \quad (2)$$

Thus, based on Equation (2), the theoretical spot size can be calculated as 13.28 mm, which is consistent with the measured result of 12.6 mm. This error of about 5% is acceptable caused by the optical path design and package. The main reason for the specific error is that in the process of packaging and debugging, in order to reduce the fine adjustment of the combined lens of the WDL, the imaging of the spot from the collimator on the LCoS-SLM is changed after passing through the optical subsystem. The input light spots from the collimator array are expanded by a 20-fold cylindrical beam expansion system, resulting in an enlarged elliptical image on the LCoS-SLM. The image is distributed by wavelength in the horizontal direction of the SLM ( $y$ -axis).

The employed LCoS chip (Holoeye Pluto) includes an array of  $1920 \times 1080$  pixels with a pitch of  $8 \mu\text{m}$  and effective length of 15.36 mm and can be addressed pixel-by-pixel. The reciprocal linear dispersion along the wavelength axis ( $y$ -axis) on the LCoS chip plane is  $0.37 \text{ GHz}/\mu\text{m}$ . That is to say, one pixel corresponds to a 3-GHz bandwidth. Thus, the minimum resolution of the central channel wavelength  $R_{\text{res\_min}}$  is 3 GHz. If a 4K LCoS-SLM is employed, the minimum resolution can be further enhanced. Theoretically, the spectral bandwidth is an integer multiple of the minimum resolution, in proportion to the number of used pixels in the  $y$ -axis. One can note that when the number of cascaded gratings increases to  $m > 5$ , the diffraction angle difference  $\Delta\Theta_m = \Theta_{\lambda_n, m} - \Theta_{\lambda_1, m} > m \cdot \Delta\Theta_1$  and the minimum resolution of the MHz scale can be theoretically achieved.

## 2.2. Implementation

In this section, the implementation and characterization of the  $1 \times 6$  programmable PSP is described.

### 2.2.1. Optical Path Design Using Zemax

In this paper, we first theoretically study the design of the compact light path based on the Gauss beam coupling equation [23]. The positions and parameters of the used optical elements are calculated. We further optimize them by using the optical path optimization and tolerancing software of Zemax as illustrated in Figure 2. This operation ensures the good coupling efficiency of the Gaussian beams from the input port couples into the multiple output ports and achieves lower values of IL. We then fix and solidify all the optical elements on an optical substrate according to the compact design in the experiment. No mechanical adjustments are needed. It is worth noting that in the optical design the beam spot size expanded by the combination of the cylindrical lenses (Components 2 and 3) matches the sizes of the two gratings, so that both gratings can be fully utilized. Meanwhile, no additional light leakage loss is introduced. The  $x$ -arises in Figure 3a,b show the normalized pupil, whose function is to represent the normalized field of view, ranging from  $-1$  to  $+1$ . As shown in Figure 3a at the wavelength direction ( $y$ -axis), the optical wavelengths of 1530 nm, 1550 nm, and 1570 nm are uniformly distributed on the LCoS plane and the simulated spot size from 1530 nm to 1570 nm is about 12.89 mm, which confirms the measured result of 12.6 mm. At the switching direction ( $x$ -axis), the spherical aberration of the optical system is optimized, and no chromatic aberration is caused for the entire C-band wavelengths, since the ray fan curves for 1530 nm, 1550 nm and 1570 nm completely coincide, as shown in Figure 3b. Furthermore, the beam spots formed by different wavelengths are well separated, as shown in Figure 3a, and the respective ellipticity of the beam spot is quite large at the switching direction, which ensures that full use is made of the LCoS pixels (approximately 400 pixels). The elliptical spots on the LCoS plane make it easier to achieve a linear optimization and high control accuracy for the signal attenuation of each wavelength (the minimum power attenuation of 0.1 dB can be achieved).

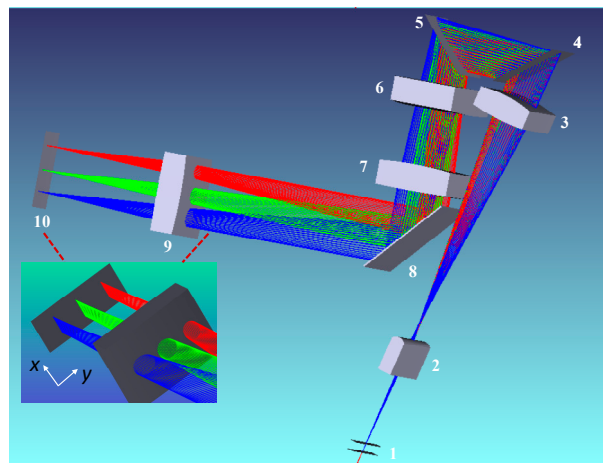


**Figure 2.** The proposed compact light path using dual-grating. The insets show the receiver beam distribution on the LCoS plane at a 45° view. The numbers 1–10 represent: No. 1 is the polarization converter with a birefringent crystal YVO<sub>4</sub> and half-wave plates; Nos. 2 and 3 are cylindrical mirrors with focal lengths of 4 mm and 60 mm, respectively; Nos. 4 and 5 are transmission gratings with 1000-line/mm resolution; Nos. 6, 7, and 9 are cylindrical lenses with focal length of 141 mm; No. 8 is a mirror; No. 10 is an LCoS chip, whose working wavelength is from 1520 nm to 1620 nm, pixel size is 8 μm, fill factor is 87% and resolution is 1920 × 1080.

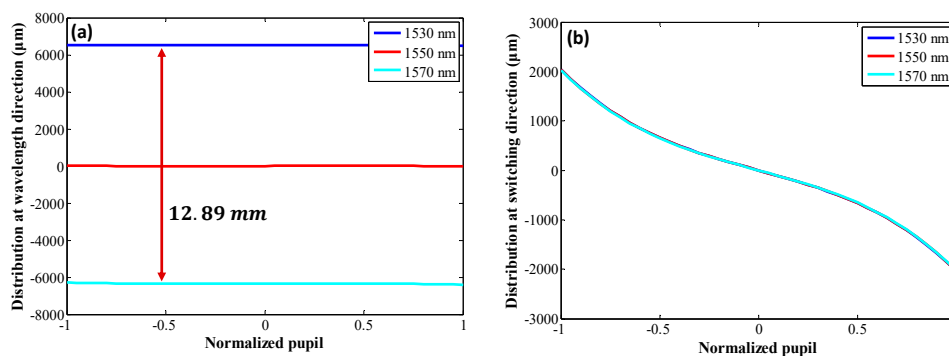


**Figure 3.** Simulation results using Zemax, (a) at the wavelength direction and (b) at the switching direction.

### 2.2.2. Experimental Setup

Figure 4 shows the experimental site of the assembled programmable PSP utilizing a compact light configuration, including a fiber array, a micro-lens array for the interaction of the light beam between the fiber and free space, a polarization conversion unit, collimating lenses, two transmission gratings, cemented lenses and a 2 K LCoS-SLM. The dense WDM optical signal from one fiber input port can be switched to several different output ports by the spectral dispersed gratings addressed on the LCoS. In the paper, one fiber port is picked as the input, and six ports with a 500 μm pitch are selected as outputs. The six output ports are divided into two groups, addressed equally on the upper and lower part of the input port. This design with symmetrical distribution helps to reduce IL differences between the output ports, because the closer the input port is to the center, the smaller the switching angle and the smaller the loss are. The beam divergence half-angle is compressed by the micro-lens array from around 0.6° to 6°. To maximally decrease the pointing error, the micro-lens array must be very carefully aligned with the input fiber array during the design process. Then, the input polarization states onto the LCoS chip are adjusted to the P-polarization, since the LCoS chip only manipulates the P-polarization light beams. A pair of cylindrical lenses are employed to collimate the beam spots and expand them into elliptical beams. The input beam further goes through the proposed light path

by using dual gratings. The cemented lens, corresponding to a lens with a focal length of 100 mm, is composed of two cylindrical lenses ( $f_1 = f_2 = 141$  mm). We add a mirror with a  $45^\circ$  reflective angle in the design to make the light path compact and more conveniently adjustable. The collimated and expanded light is finally converged on the LCoS display and modulated by its phase grating. Different optical spectra are projected onto different pixels of the LCoS chip plane. The diffracted and reflected spectra are recombined again by the transmission gratings onto the individual output ports. Thus, light beams with different wavelengths are able to be routed to any desired output ports.

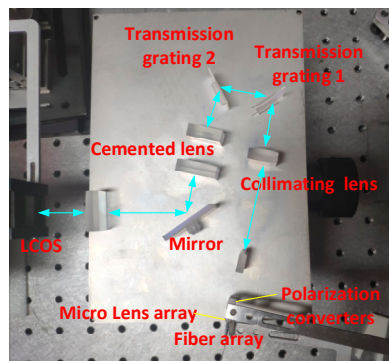


**Figure 4.** Experimental site using our proposed low-cost compact spatial light paths. All the optical elements are solidified on an optical substrate.

### 3. Experimental Results and Discussions

We first measured the IL of each output port as a function of the input wavelength across the whole C-band. In the experiment, a scanning laser source module (Agilent, 81940A) with a sweeping step of 0.001 nm is employed as a transmitter whose wavelength range is set from 1530 nm to 1570 nm. At the receiver side, we use a high-sensitivity optical power meter module (Agilent, N7745A) to detect the optical spectra one by one. According to the measured results as shown in Figure 5, the total IL fluctuations for the six output ports are between 5.9 dB to 9.4 dB, corresponding to port 1 and port 4. The introduced IL can be mainly classified as static loss and dynamic loss [24]. The former one is mainly caused by optical components such as the two transmission gratings (1.9 dB), micro-lens array (1.5 dB), LCoS chip (0.9 dB), collimating lens (0.5 dB), polarization conversion unit (0.5 dB), and cylindrical lens (0.2 dB). These ILs are calculated according to the corresponding material parameters. Due to the input and output of the optical path and the record of passing twice, these losses are doubled in the calculation. The latter one is mainly induced by different responses of different wavelengths passing through the slanted cascaded transmission gratings and different distances between the principal optical axis and output ports, leading to fluctuation losses from 0.4 dB to 3.9 dB. For each port, the measured intrinsic WDL within the full C-band is around 1 dB as illustrated in Figure 5.

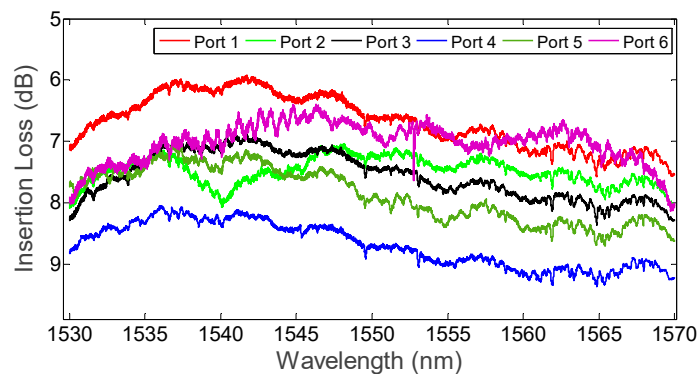


**Figure 5.** Measured total insertion loss (IL) for six ports in the full C-band wavelengths.

In order to facilitate the programming of the spectrum, we have written the corresponding operation software, and its operation interface is similar to that of Finisar WaveShaper. After calibrating the LCoS-SLM grayscale of the corresponding device port, and the accuracy of the wavelength and pixel control bandwidth, our software can also directly read the .txt or .xlsx data files composed of the wavelength, port and attenuation along the whole C-band, so as to realize the programming on the wavelength.

In the following measured results illustrated in Figures 6–9, we choose port 3 with neither the maximum nor the minimum IL of the C-band as the representative of the research object. Figure 6 shows the measured flexible 3-dB bandwidth adjustments from 6.2 GHz to 25.3 GHz by increasing the number of pixels on the LCoS chip one-by-one across the  $y$ -axis. The starting position is selected at the center of all the covered LCoS pixels, corresponding to the wavelength of 1550.8 nm. Without introducing extra IL, the achieved minimum 3-dB bandwidth is 9.8 GHz as shown in Figure 6. The maximum bandwidth can be extended to 5 THz across the entire C-band by adjusting a step of about 3.1 GHz, which is consistent with the theoretical minimum resolution of 3 GHz. The minimum filtering bandwidth of 6.2 GHz (corresponding to one pixel) can be obtained by introducing a 9-dB extra loss, since a fewer number of pixels results in a higher optical power loss. When increasing the 3-dB bandwidth to 8.1 GHz, the extra loss is decreased to 1.4 dB. We also measured the minimum 3-dB bandwidths in the C-band at the central wavelengths of 196 THz (1529.553 nm), 195 THz (1537.397 nm), 194 THz (1545.322 nm), 193 THz (1553.329 nm), 192 THz (1561.419 nm) and 191 THz (1569.594 nm), respectively. As illustrated in Figure 7, the measured values are about 8.4 GHz, 8.1 GHz, 6.7 GHz, 6.59 GHz, 6.9 GHz and 7 GHz, corresponding to side band suppression ratios of 27 dB, 28 dB, 31 dB, 31.1 dB, 31.3 dB, and 29.3 dB, respectively.

Furthermore, a programmable PSP needs to possess the capability to arbitrarily attenuate the optical power in order to meet the special spectral requirement. In the experiment, by using our proposed PSP, we generate three sets of continuous sine waves with repetition frequencies of 2.5 GHz (0.02 nm), 0.25 GHz (0.002 nm), and 0.125 GHz (0.001 nm), respectively. As shown in Figure 8, the achieved peak-to-peak power suppressions for 2.5 GHz, 0.25 GHz and 0.125 GHz sine waves are 23.4 dB, 18 dB and 6 dB, respectively. The experimental results show that when the frequency interval is greater than or equal to 0.25 GHz, our proposed system can already produce a peak-to-peak power suppression signal greater than 18 dB, and the performance is good. In addition, in order to further verify the application of our method in communications such as OFDM, we have also produced OFCs with spacing of 12.5 GHz and 25 GHz.

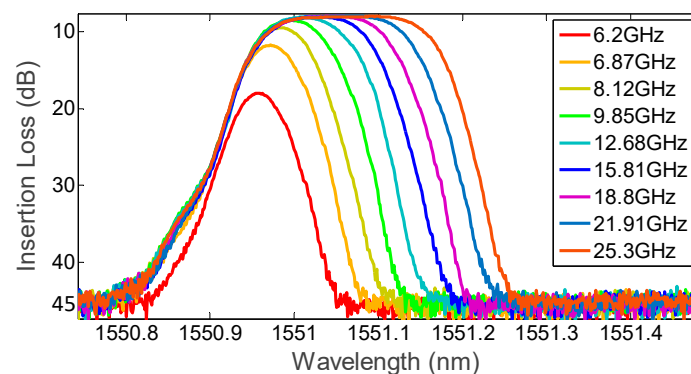


**Figure 6.** Flexible bandwidth adjustment with a minimum 3-dB bandwidth of 6.2 GHz to 25.3 GHz.

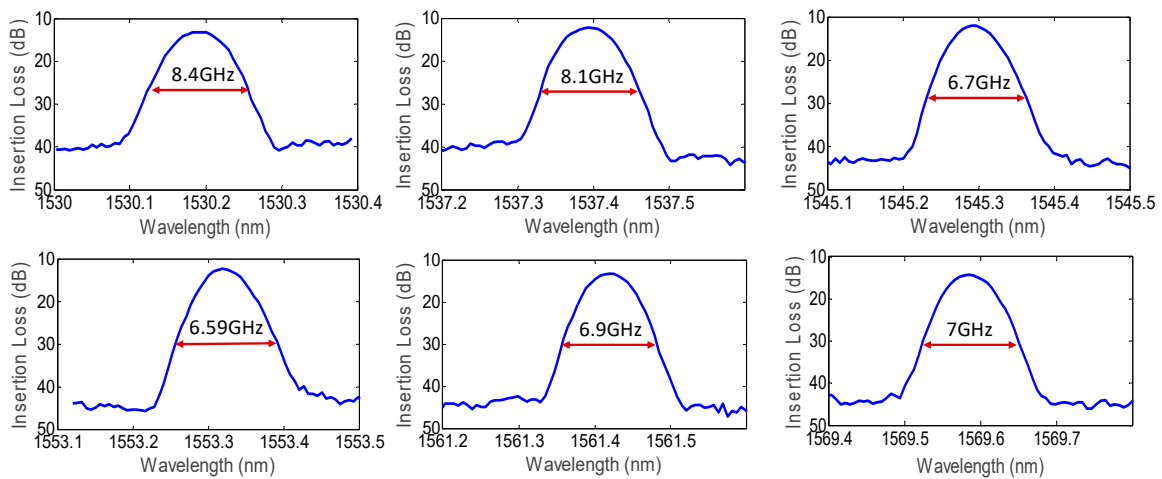


**Figure 7.** Measured minimum bandwidths in the C-band at the central wavelengths of 196 THz (1529.553 nm), 195 THz (1537.397 nm), 194 THz (1545.322 nm), 193THz (1553.329 nm), 192 THz (1561.419 nm) and 191 THz (1569.594 nm), respectively.

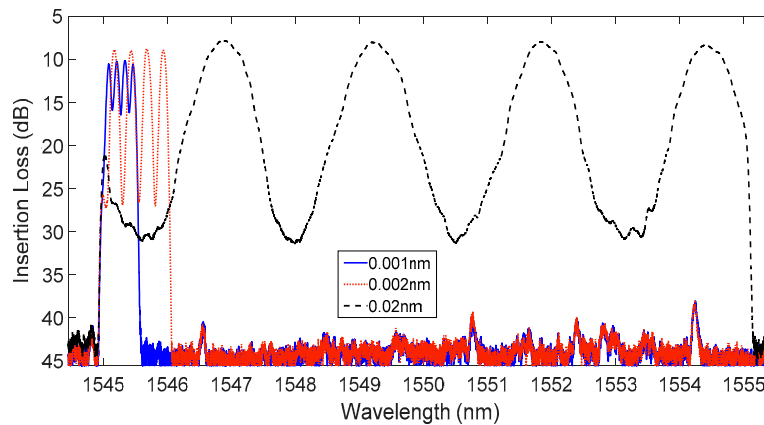


**Figure 8.** Measured optical spectra for 2.5 GHz (0.02 nm), 0.25 GHz (0.002 nm), and 0.125 GHz (0.001 nm) continuous sine waves.

Figure 9a shows the measured spectral results of 12.5 GHz and 25 GHz combs by using our designed  $1 \times 6$  PSP, and the peak-to-peak power suppressions are more than 8 dB and 25 dB, respectively. Figure 9b shows the measured spectral results of 12.5 GHz and 25 GHz combs by using a commercial PSP, whose peak-to-peak power suppressions are about 3 dB and 18.7 dB, respectively. Obviously, the performance of our proposed system outperforms that of commercial PSP. This is due to the stronger ability by the proposed method to distinguish photons to the output ports.

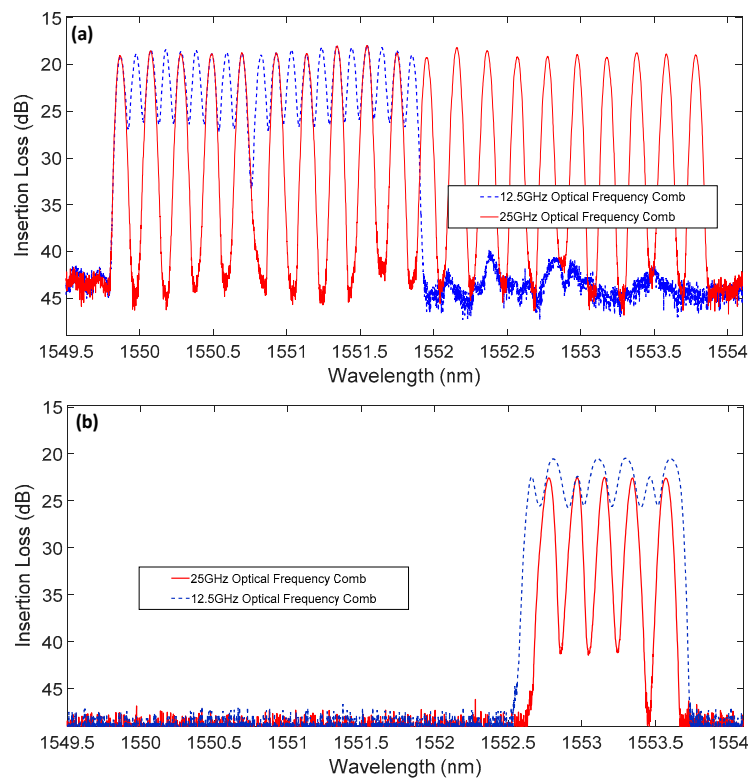


**Figure 9.** Measured spectra of optical frequency combs (OFCs) with 12.5 GHz and 25 GHz space using (a) our  $1 \times 6$  PSP and (b) commercial PSP.

#### 4. Conclusions

In this paper, we have developed a fine-resolution programmable PSP based on low-cost compact light paths, enabled by a 2K LCoS-SLM and dual cascaded 1000 line/mm diffraction gratings. An assembled experimental system with one-input and six-output has been built in order to implement a flexible filtering bandwidth and arbitrary amplitude transfer function. The measured total ILs for the six ports are around 5.9 dB–9.4 dB over the full C-band. The achieved minimum 3-dB bandwidth is 6.2 GHz, and the largest operating bandwidth can be extended to the full C-band from 1530 nm to 1570 nm (5 THz). Moreover, by using the proposed PSP, a high-resolution high-performance arbitrary optical spectrum can be generated, such as a sine wave signal with a 0.25-GHz repetition frequency and 18-dB peak-to-peak power suppression. Based on the achieved experimental results, developing a programmable and high-resolution  $1 \times N$  PSP by using low-cost compact spatial light paths is feasible, and is believed to further the implementation of an  $M \times N$  PSP.

**Author Contributions:** Z.L. performed the investigation and experiment, wrote the original draft; C.L. performed the analytical calculations and revised the manuscript; J.T. discussed with the experimental results and revised the manuscript; S.Y. supervised the whole project and approved the manuscript. All authors have read and agreed to the published version of the manuscript.

**Funding:** This work was supported by National Natural Science Foundation of China (61805184), Hubei Provincial Natural Science Foundation of China (2018CFB250), Anhui Provincial Natural Science Foundation of China (1808085MF186).

**Acknowledgments:** The first author would like to thank Quan You, Ying Qiu and Xi Xiao from National Information Optoelectronics Innovation Center, Wuhan Research Institute of Posts and Telecommunications, for useful discussions during the experiment. And also thank Fulong Yan from Eindhoven University of Technology for valuable suggestions.

**Conflicts of Interest:** The authors declare no conflict of interest.

## References

1. Zhang, J.; Yu, J.; Zhu, B.; Li, F.; Chien, H.; Jia, Z.; Cai, Y.; Li, X.; Xiao, X.; Fang, Y.; et al. Transmission of single-carrier 400G signals (515.2-Gb/s) based on 128.8-GBaud PDM QPSK over 10,130-and 6,078 km terrestrial fiber links. *Opt. Express* **2017**, *23*, 16540–16545. [[CrossRef](#)]
2. Marom, D.M.; Colbourne, P.D.; D’Errico, A.; Fontaine, N.K.; Ikuma, Y.; Proietti, R.; Zong, L.; Moscoso, J.; Tomkos, I. Survey of photonic switching architectures and technologies in support of spatially and spectrally flexible optical networking. *J. Opt. Commun. Netw.* **2017**, *9*, 1. [[CrossRef](#)]
3. Chandrasekhar, S.; Liu, X. OFDM based superchannel transmission technology. *IEEE/OSA J. Lightwave Technol.* **2012**, *30*, 3816–3823. [[CrossRef](#)]
4. Xiang, M.; Fu, S.; Tang, M.; Taang, H.; Shum, P.; Liu, D. Nyquist WDM superchannel using offset-16QAM and receiver-side digital spectral shaping. *Opt. Express* **2014**, *22*, 17448. [[CrossRef](#)] [[PubMed](#)]
5. Woodward, S.L.; Feuer, M.D. Benefits and requirements of flexible-grid ROADMs and networks. *J. Opt. Commun. Netw.* **2013**, *5*, A19. [[CrossRef](#)]
6. Li, Y.; Zong, L.; Gao, M.; Mukherjee, B.; Shen, G. Colorless, partially directional, and contentionless architecture for high-degree ROADMs. In Proceedings of the Optical Fiber Communications Conference and Exhibition (OFC), San Diego, CA, USA, 8–12 March 2020; IEEE: Piscataway, NJ, USA, 2020; p. M4D.2.
7. Yang, H.; Dolan, P.; Robertson, B.; Wilkinson, P.; Chu, D. Crosstalk spectrum optimisation for stacked wavelength selective switches based on 2D beam steering. In Proceedings of the Optical Fiber Communications Conference and Exhibition (OFC), San Diego, CA, USA, 11–15 March 2018; IEEE: Piscataway, NJ, USA, 2018; p. Th1J.2.
8. Wilkinson, P.; Robertson, B.; Giltrap, S.; Snowdon, O.; Prudden, H.; Yang, H.; Chu, D.  $241 \times 12$  wavelength-selective switches using a 312-port 3D waveguide and a single 4k LCoS. In Proceedings of the Optical Fiber Communications Conference and Exhibition (OFC), San Diego, CA, USA, 8–12 March 2020; IEEE: Piscataway, NJ, USA, 2020; p. M3F.2.
9. Ma, Y.; Clarke, I.; Stewart, L. Recent progress on wavelength selective switch. In Proceedings of the Optical Fiber Communications Conference and Exhibition (OFC), San Diego, CA, USA, 8–12 March 2020; IEEE: Piscataway, NJ, USA, 2020; p. M3F.1.
10. Sorimoto, K.; Tanizawa, K.; Uetsuka, H.; Kawashima, H.; Mori, M.; Hasama, T.; Ishikawa, H.; Tsuda, H. Compact and phase-error-robust multilayered AWG-based wavelength selective switch driven by a single LCoS. *Opt. Express* **2013**, *24*, 17131–17149. [[CrossRef](#)] [[PubMed](#)]
11. Robertson, B.; Yang, H.; Redmond, M.; Collings, N.; Moore, J.R.; Liu, J.; Jeziorska-Chapman, A.M.; Pivnenko, M.; Lee, S.A.; Wonfor, I.H.; et al. Demonstration of multi-casting in a  $1 \times 9$  lcos wavelength selective switch. *IEEE/OSA J. Lightwave Technol.* **2014**, *32*, 402. [[CrossRef](#)]
12. Iwama, M.; Takahashi, M.; Kimura, M.; Uchida, Y.; Hasegawa, J.; Hara, R.K.; Kagi, N. LCoS-based flexible grid  $1 \times 40$  wavelength selective switch using planar lightwave circuit as spot size converter. In Proceedings of the Optical Fiber Communications Conference and Exhibition (OFC), Los Angeles, CA, USA, 22–26 March 2015; IEEE: Piscataway, NJ, USA, 2015; p. Tu3A.8.
13. Lu, T.; Collings, N.; Robertson, B.; Chu, D. Design of a low-cost and compact  $1 \times 5$  wavelength-selective switch for access networks. *OSA Appl. Opt.* **2015**, *54*, 8844–8855. [[CrossRef](#)] [[PubMed](#)]
14. Xie, D.; Wang, D.; Zhang, M.; Liu, Z.; You, Q.; Yang, Q.; Yu, S. LCoS-based wavelength-selective switch for future finer-grid elastic optical networks capable of all-optical wavelength conversion. *IEEE Photonics J.* **2017**, *9*, 7101212. [[CrossRef](#)]
15. Gao, Y.; Chen, G.; Chen, X.; Zhang, Q.; Chen, Q.; Zhang, C.; Tian, K.; Tan, Z.; Yu, C. High-resolution tunable filter with flexible bandwidth and power attenuation based on an LCoS processor. *IEEE Photonics J.* **2018**, *10*, 6. [[CrossRef](#)]
16. Gao, Y.; Chen, X.; Chen, G.; Tan, Z.; Chen, Q.; Dai, D.; Zhang, Q.; Yu, C. Programmable spectral filter in C-Band based on digital micromirror device. *Micromachines* **2019**, *10*, 163. [[CrossRef](#)] [[PubMed](#)]
17. Rudnick, R.; Tolmachev, A.; Sinefeld, D.; Golani, O.; Ben-Ezra, S.; Nazarathy, M.; Marom, D.M. Sub-GHz resolution photonic spectral processor and its system applications. *IEEE/OSA J. Lightwave Technol.* **2017**, *35*, 2218. [[CrossRef](#)]
18. Xie, D.; Liu, Z.; You, Q.; Yu, S. Demonstration of a  $3 \times 4$  tunable bandwidth WSS with tunable attenuation using compact spatial light paths. *Opt. Express* **2017**, *25*, 11173. [[CrossRef](#)] [[PubMed](#)]

19. Fontaine, N.K.; Ryf, R.; Neilson, D.T.  $N \times M$  wavelength selective crossconnect with flexible passbands. In Proceedings of the Optical Fiber Communications Conference and Exhibition (OFC), Los Angeles, CA, USA, 4–8 March 2012; IEEE: Piscataway, NJ, USA, 2011; p. PDP5B.2.
20. Xiao, F.; Alameh, K. Opto-VLSI-based  $N \times M$  wavelength selective switch. *OSA Opt. Express* **2013**, *21*, 18160. [[CrossRef](#)] [[PubMed](#)]
21. Lbsen Photonics, PING-Sample-083. Available online: <https://ibsen.com/products/transmission-gratings/ping-telecom-%20gratings/telecom-c-band-gratings/ping-sample-083/> (accessed on 5 December 2020).
22. Palmer, C.A.; Loewen, E.G. *Diffraction Grating Handbook*; Thermo RGL: New York, NY, USA, 2002.
23. Born, M.; Wolf, E. Principles of optics: Electromagnetic theory of propagation, interference and diffraction of light. *Phys. Today* **2000**, *53*, 77. [[CrossRef](#)]
24. Wang, M.; Zong, L.; Mao, L.; Marquez, A.; Ye, Y.; Zhao, H.; Vaquero, F.J. LCoS SLM study and its application in wavelength selective switch. *Photonics* **2017**, *4*, 22. [[CrossRef](#)]

**Publisher’s Note:** MDPI stays neutral with regard to jurisdictional claims in published maps and institutional affiliations.



© 2020 by the authors. Licensee MDPI, Basel, Switzerland. This article is an open access article distributed under the terms and conditions of the Creative Commons Attribution (CC BY) license (<http://creativecommons.org/licenses/by/4.0/>).